Preprint typeset using LaTeX style emulateapj v. 6/22/04

CONSTRAINING GRB INITIAL LORENTZ FACTOR WITH THE AFTERGLOW ONSET FEATURE AND DISCOVERY OF A TIGHT $\Gamma_0 - E_{\gamma,\rm ISO}$ CORRELATION

En-Wei Liang[1,3], Shuang-xi Yi[1], Jin Zhang[2], Hou-Jun Lü [1], Bin-Bin Zhang[3], and Bing Zhang[3]

ABSTRACT

The onset of GRB afterglow is characterized by a smooth bump in the early afterglow lightcurve caused by the deceleration of the gamma-ray burst (GRB) fireball by the circumburst medium. We make an extensive search for such a deceleration feature, either from the literature for optical lightcurves, or from the X-ray afterglow lightcurve catalog established with the Swift/XRT. Twenty optically selected GRBs and 12 X-ray selected GRBs are found to show the onset signature, among which 17 optically selected GRBs and 2 X-ray-selected GRBs have redshift measurements. We study the optical z-known sample by fitting the lightcurves with a smooth broken power-law and measure the width (w), rising timescale (t_r), and decaying timescale (t_d) at full-width-at-half-maximum (FWHM). Strong mutual correlations among these timescales and with the peak time (t_p) are found. The optical peak luminosity ($L_{\rm p,O}$) at the lightcurve bump is anti-correlated with t_p and correlated with w, indicating a dimmer and broader bump at a later peak time. The ratio t_r/t_d is almost universal among bursts, but the ratio t_r/t_p varies from $0.3 \sim 1$. The isotropic gamma-ray energy ($E_{\gamma,\rm iso}$) is tightly correlated with $L_{\rm p,O}$ and t_p in the burst frame. Assuming that the bumps signal the deceleration of the GRB fireballs in a constant density medium, we calculate the initial Lorentz factor (Γ_0) and the deceleration radius ($R_{\rm d}$) of the GRBs in the optical-selected sample. It is found that Γ_0 are typically a few hundreds, and the typical deceleration radius is $R_{\rm dec} \sim 10^{17}$ cm. More intriguingly, a tight correlation between the initial Lorentz factor and the isotropic gamma-ray energy is found, namely $\Gamma_0 \simeq 195 E^{0.27}_{\gamma,\rm iso,52}$ (satisfied for both the optical and X-ray z-known samples). This correlation is helpful to understand GRB physics, and may serve as an indicator of Γ_0 for other long GRBs. We find that the early bright X-rays are usually dominated by a different component from the external shock emission, but occasionally (for one case) an achromatic deceleration feature is observed. Components in X-rays would contribute to the diversity of the observed X-ray lightcurves.

Subject headings: radiation mechanisms: non-thermal: gamma-rays: bursts

1. INTRODUCTION

The fireball model has been extensively employed to explain the gamma-ray burst (GRB) phenomenon (Mészáros 2002; Zhang & Mészáros 2004; Piran 2004). The observed prompt gamma-ray emission is explained by synchrotron (or inverse Compton) emission from the internal shocks in an erratic, unsteady, relativistic fireball (Rees & Mészáros 1994), and broadband afterglow emission is attributed to synchrotron emission from the external shock when the fireball is decelerated by a circumburst medium (Mészáros & Rees 1997; Sari et al. 1998). In order to avoid the "compactness problem" of high energy non-thermal photons detected from GRBs, the GRB fireball is required to move relativistically towards earth. After the initial radiation-dominated acceleration phase, the fireball enters the matter-dominated "coasting" phase. The fireball keeps an approximately same Lorentz factor until it sweeps up a considerable amount mass from the ambient medium at the so-called deceleration radius, after which Γ decreases with R (and the observer time t) as a power law. The factor Lorentz factor during the coasting phase is called the initial Lorentz factor (Γ_0), which is a crucial parameter to understand GRB physics, but is poorly known for most GRBs.

Three methods have been proposed to measure the initial Lorentz factor Γ_0. The first method is to apply the "compactness" argument to use the high energy photon cutoff energy in the GRB prompt emission spectrum to estimate Γ_0. Since so far no clear cutoff feature is observed, the common practice is to use the observed maximum photon energy to set a lower limit on Γ_0 (Fenimore et al. 1993; Woods & Loeb 1995; Baring & Harding 1997; Lithwick & Sari 2001). This method suffers several uncertainties. First, the cutoff energy depends on both Γ_0 and the emission radius R_γ (Gupta & Zhang 2008). The method therefore relies on the assumption of $R_\gamma = \Gamma_0^2 c\delta t$, the internal shock radius. Such an assumption is not necessarily correct. Second, the minimum variability time scale δt is subject to large uncertainty, since the GRB lightcurves are chaotic and do not have a characteristic time scale. Finally, Fermi observations (Abdo et al. 2009b,c) indicate that some GRBs have a distinct high energy component in the GeV range, which may come from a different emission region. A straightforward usage of the method may lead to erroneous conclusions. The second method to measure Γ_0 is to use the blackbody component detected in some GRB spectra (Pe'er et al. 2007). The limitation of the method is the difficulty of identifying blackbody components from the GRB spectra. So far the only case that this method is securely applied is GRB 090902B (Ryde et al. 2009). The third, but most commonly adopted, method is to use

[1] Department of Physics, Guangxi University, Nanning 530004, China; lew@gxu.edu.cn
[2] College of Physics and Electronic Engineering, Guangxi Teachers Education University, Nanning, Guangxi, 530001, China
[3] Department of Physics and Astronomy, University of Nevada, Las Vegas, NV 89154. zhang@physics.unlv.edu

the early afterglow lightcurve. The fireball model predicts that at the onset of deceleration, the emission from the forward shock would display a smooth bump in the lightcurve, the peak of which corresponds to the epoch when essentially half of the fireball energy is transferred to the medium (Sari & Piran 1999; Kobayashi & Zhang 2007). The most relevant case is the thin shell regime, defined by that the thickness of the fireball shell satisfies $\Delta < (E/nm_pc^2)^{1/3}\Gamma_0^{-8/3}$, where E is the kinetic energy of the fireball, n is the medium density, m_p the mass of proton, c speed of light (Kobayashi et al. 1999; Sari & Piran 1999). Within this regime, the deceleration time (the peak time at the lightcurve bump, $t_p \propto \Gamma_0^{-8/3}(E/n)^{1/3}$, Mészáros & Rees 1993) is sensitive depends on the initial Lorentz factor but insensitive to other parameters. The detection of this time can be then used to infer Γ_0. In the optical band, early emission may be contaminated by the emission from the reverse shock (Mészáros & Rees 1997; Sari & Piran 1999; Kobayashi 2000; Zhang et al. 2003). However, under certain conditions (either a Poynting flux dominated flow, Zhang & Kobayashi 2005; or a relatively low typical synchrotron frequency in the reverse shock, Jin & Fan 2007), the reverse shock component would not show up in the optical band. In these bursts, a smooth onset bump can be detected, which signals the deceleration feature of the fireball, and hence, can be used to constrain the initial Lorentz factor and the deceleration radius (Sari Piran 1999, Zhang et al. 2003; Molinari et al. 2007; Xue et al. 2009; Zou & Piran 2009).

In this paper, we constrain Γ_0 with the early GRB afterglows that show the deceleration signature, and investigate the possible correlations among deceleration parameters (including Γ_0) as well as the prompt gamma-ray emission properties. We make an extensive search for the onset of afterglow signature in the optical and X-ray lightcurves. Our sample selection is presented in Section 2. The temporal characteristics and their correlations are presented in Section 3, and the relation between the prompt gamma-ray properties and the deceleration properties are investigated in Section 4. In particular, we constrain Γ_0 and the deceleration radius of the fireball for the z-known sample, and discover a tight correlation between Γ_0 and $E_{\gamma,\rm iso}$. Discussion and conclusions are presented in Sections 5 and 6, respectively. A concordance cosmology with parameters $H_0 = 71$ km s^{-1} Mpc^{-1}, $\Omega_M = 0.30$, and $\Omega_\Lambda = 0.70$ are adopted. Notation Q_n denotes $Q/10^n$ in the cgs units throughout the paper.

2. SAMPLE SELECTION AND LIGHTCURVE FITTING

We make an extensive search for the smooth "bump" feature as the onset of GRB afterglow. The flares or the reversed shock emission component introduce confusion to identify the onset feature, especially in the X-ray band. We therefore employ the following two criteria to selection the samples. First, the bump is smooth without superimposing significant flares around the bump. Second, the decay slopes post the peak time is shallower than -2. Through literature search, we obtain 20 optical-selected GRBs that show the afterglow onset feature. We also go through the Swift XRT lightcurve archive that has been processed by our group in the past (from January 2005 to September 2009), and identify 12 X-ray selected sample with afterglow onset signature. The observational results of these bursts are summarized in Tables 1 and 2. The details of XRT data reduction have been presented in a series of papers published by our group (Zhang et al. 2007a, Paper I; Liang et al. 2007, 2008, 2009; Papers II, III, IV). The prompt gamma-ray properties of the bursts are taken from the published papers or GCN reports.

The afterglow lightcurves of the optical-selected and the X-ray-selected samples are presented in Figures 1 and 2, respectively. The early X-ray afterglow lightcurves for the optical-selected sample, and the optical afterglow lightcurves for the X-ray selected sample are also present, if they are available. In the X-ray selected sample, only few cases have simultaneous optical observation. Nineteen out of 20 GRBs in the optical-selected sample have simultaneously X-ray observations. We find only one case, GRB 080319C, that shows a clear achromatic onset bump in both the optical and X-ray bands. This suggests that the external shock emission indeed contributes to both the optical and the X-ray band. For most optical-selected sample GRBs, on the other hand, the early X-ray lightcurves either show erratic X-ray flares or internal plateaus that are believed to be powered by the GRB central engine, or the X-ray observations started only after the optical bump peak. Inspecting the two samples shown in Figures 1 and 2, we find that the onset bumps in the optical-selected sample are usually smoother than those observed in the X-ray-selected sample. Seventeen out of the 20 GRBs in the optical-selected sample and two out of 12 GRBs in the X-ray-selected sample have redshift measurements. In the following, we mostly use only the z-known optical-selected sample in our analysis but will use the z-known X-ray-selected sample to confirm the findings.

We fit the lightcurves with an empirical model proposed by Kocevski & Liang (2001),

$$F(t) = F_p(\frac{t+t_0}{t_p+t_0})^r[\frac{d}{r+d} + \frac{r}{r+d}(\frac{t+t_0}{t_p+t_0})^{r+1}]^{-\frac{r+d}{r+1}}, \quad (1)$$

where F_p is the maximum flux at t_p, t_0 is a reference time, and r and d are the rising and decaying power-law indices, respectively. An IDL routine called *mpfitfun.pro* is employed for our fitting. This routine performs Levenberg-Marquardt least-square fit to the data for a given model. It optimizes the model parameters so that the sum of the squares of the deviations between the data and the model becomes minimal. The time interval and the fitting curve for each GRB are shown in Figures 1 and 2, and the fitting parameters are summarized in Tables 1 and 2 [4]. Notice that the lightcurves of some GRBs, such as 050820A, 060607A, 070411, 071031, 080330, show significant energy injection or re-brightening features after the deceleration bump. We make our fits only around the bump. Our fits are also shown in Figures 1 and 2.

3. CHARACTERISTICS OF THE ONSET BUMP AND THEIR CORRELATIONS

For each fitting lightcurve, we take the full-width-at-half-maximum (FWHM) as a characteristic width (w) of the bump, and measure the rising and decaying

[4] The reduced χ^2 of our fits for some optical lightcurves are large. This is due to the fluctuations in the lightcurves and small observational errors in the optical data.

timescales (t_r and t_d) at FWHM. We also derive the ratios of t_r/t_p and t_r/t_d. The results are reported in Tables 1 and 2. The distributions of r, d, t_p,t_r, t_d, F_p, w, t_r/t_p, and t_r/t_d are shown in Figure 3.

The following statistics applies to the optical-selected sample. As shown in Figure 3, the rising index r of most bursts are in the range of $1-2$, with three exceptional cases, i.e., GRBs 080330 ($r = 0.34 \pm 0.03$), 060607A ($r = 4.15 \pm 0.22$), and 050820A (4.45 ± 0.76). Inspecting the optical lightcurve of GRB 080330, the optical flux increases slowly, keeping almost a constant in $300-1000$ seconds post the GRB trigger. This feature is similar to that observed in GRB 060614. For GRBs 060607A, and 050820A, their optical lightcurves show a similar behavior, with rapid increase prior to the peak and a normal decay post the peak. The decaying index d is distributed in the range of $0.44-1.77$, with a mean value 1.16 ± 0.34. Except for GRBs 080330 and 061007, the decay indices are well consistent with the isotropic forward shock models in a constant density medium. The decay indices of the two exceptions are ~ 1.7, slightly steeper than the normal decay slope predicted by the isotropic forward shock models. The t_p is in the range of 10^2-10^3 seconds with a median value ~ 380 seconds. The distribution of F_p ranges in $10^{-13}-10^{-8}$ ergs cm^{-2} s^{-1}, with a mean 7.25×10^{-12} erg cm^{-2} s^{-1}. The width w is distributed in 10^2-10^3 seconds. The t_r and t_d peak around 10^2 seconds and 10^3 seconds, respectively. The ratio t_r/t_d is narrowly distributed in $0.1-0.3$. However, the distribution of the ratio t_r/t_p is much wider, ranging in $0.3-1$.

We show various correlations among the deceleration parameters of the optical selected sample in Fig. 4, and summarize the linear correlation coefficients from pair Spearman correlation analysis in Table 3. Tight correlations are found among t_r, t_d, t_p and w. The coefficients of these correlations are larger than 0.93. These correlations are

$$\log t_d = (0.48 \pm 0.13) + (1.06 \pm 0.06) \log t_r \quad (2)$$

$$\log t_d = (-0.09 \pm 0.29) + (1.17 \pm 0.11) \log t_p \quad (3)$$

$$\log t_r = (-0.54 \pm 0.22) + (1.11 \pm 0.08) \log t_p \quad (4)$$

$$\log w = (0.05 \pm 0.27) + (1.16 \pm 0.10) \log t_p \quad (5)$$

$$\log w = (0.61 \pm 0.11) + (1.05 \pm 0.05) \log t_r \quad (6)$$

$$\log w = (0.15 \pm 0.02) + (0.98 \pm 0.01) \log t_d. \quad (7)$$

The tight $t_r - t_d$ correlations suggest that the structure of the bumps among bursts are similar, indicating a universal physical origin. No correlation of the decay index d with the other parameters is found. This is consistent with the expectation of blastwave model, in which the decay slope is dictated by the density profile and the electron spectral index p but has nothing to do with the afterglow onset details. On the other hand, the rising index r is tightly anti-correlated with both the ratio t_r/t_d and t_r/t_p, although it is not correlated with t_r and t_d. These correlations read

$$\log r = (-0.21 \pm 0.06) - (1.68 \pm 0.19) \log t_r/t_p \quad (8)$$

$$\log r = (-0.15 \pm 0.02) - (0.48 \pm 0.05) \log t_r/t_d. \quad (9)$$

The $w - t_p$ correlation indicates that the wider bumps tend to peak at a later time. In addition, both w and t_p in the burst frame are anti-correlated with the peak luminosity at the bump peak $L_{\rm p,O}$,

$$\log L_{\rm p,O} = (54.6 \pm 0.8) - (2.48 \pm 0.38) \log t_p^{'} \quad (10)$$

$$\log L_{\rm p,O} = (0.82 \pm 0.79) - (2.16 \pm 0.31) \log w^{'}. \quad (11)$$

These results suggest that a dimmer bump tends to peak at a later time with a longer duration.

4. INITIAL LORENTZ FACTOR CONSTRAINTS AND THE $\Gamma_0 - E_{\gamma,\rm ISO}$ CORRECTION

The observation properties of the early optical bumps seem to be consistent with being due to the onset of the external shock afterglow in the thin shell regime. To test this hypothesis, we check the correlations of $L_{p,O}$ and the cosmic-frame peak time $t_{p,z} = t_p/(1+z)$ with the isotropic gamma-ray energy $E_{\gamma,\rm iso}$ in Figure 5. We find that they are strongly correlated, i.e.

$$\log L_{\rm p,O} = (47.10 \pm 0.12) + (1.17 \pm 0.13) \log E_{\gamma,\rm iso,52} \quad (12)$$

$$\log t_{\rm p,z} = (2.25 \pm 0.07) - (0.38 \pm 0.07) \log E_{\gamma,\rm iso,52} \quad (13)$$

with a correlation coefficient $\kappa = 0.88$ and chance probability $< 10^{-4}$ for both correlations. We also derive the isotropic optical energy release from 10 seconds to 10^5 seconds post the GRB trigger ($E_{\rm O,iso}$) using the fitting curves, and show the correlation between $E_{\rm O,iso}$ and $E_{\gamma,\rm iso}$ in Figure 5. This correlation, i.e.

$$\log E_{\rm p,O} = (49.63 \pm 0.09) + (0.74 \pm 0.10) \log E_{\rm iso,52} \quad (14)$$

has a correlation coefficient $\kappa = 0.89$ and chance probability $< 10^{-4}$.

These tight correlations indicate that a GRB with a larger $E_{\gamma,\rm iso}$ tends to have a brighter optical afterglow peaking at an earlier time. This is well consistent with the afterglow onset theory. The shape of the lightcurve is consistent with the thin shell case (cf. the thick shell case, see Kobayashi et al. 1999; Kobayashi & Zhang 2007). We therefore apply the standard afterglow model in a constant density medium (Sari & Piran 1999) to derive the initial Lorentz factor

$$\Gamma_0 = 2\left[\frac{3E_{\gamma,\ \rm iso}}{32\pi n m_p c^5 \eta t_{\rm p,z}^3}\right]^{1/8} \simeq 193 (n\eta)^{-1/8} \times \left(\frac{E_{\gamma,\rm iso,52}}{t_{\rm p,z,2}^3}\right)^{1/8}, \quad (15)$$

and the deceleration radius

$$R_{\rm dec} = 2ct_p\Gamma_p^2/(1+z) = 2.25\times10^{16}{\rm cm}\ \Gamma_{0,2}^2 t_{p,z,2}, \quad (16)$$

where $\eta = E_{\gamma,\rm iso}/E_{\rm K,iso}$ is the ratio between the isotropic gamma-ray energy and the isotropic blastwave kinetic energy. The results are rather insensitive to n and η. In the following analysis, we take $n = 1$ cm^{-3} and $\eta = 0.2$ throughout.

With the data reported in Table 1, we calculate Γ_0 and $R_{\rm dec}$ for the GRBs in the optical-selected sample. The results also reported in Table 4. The distributions of the derived Γ_0 and $R_{\rm dec}$ are displayed in Fig. 6. We can see that Γ_0 is typically a few hundreds, and the typical deceleration radius is $R_{\rm dec} = 1\times10^{17}$. From Eq. 15, we find Γ_0 depends on both $t_{p,z}$ and $E_{\rm iso}$. As $t_{p,z}$ is tightly correlated with $E_{\rm iso}$, one expects tight relations between Γ_0 and $E_{\gamma,\rm iso}$ and between Γ_0 and $t_{p,z}$. We show the two relations in Figure 7. The best fits give

$$\log \Gamma_0 = (3.69 \pm 0.09) - (0.63 \pm 0.04) \log t_{\rm p,z} \quad (17)$$

with the correlation coefficient $\kappa = -0.97$ (chance probability $p < 10^{-4}$) and

$$\log \Gamma_0 = (2.291 \pm 0.002) + (0.269 \pm 0.002) \log E_{\gamma,\rm iso,52} \quad (18)$$

with correlation coefficient $\kappa = 0.91$ (chance probability $< 10^{-4}$). These tight correlations suggest that $t_{p,z}$ and $E_{\gamma,\rm iso}$ are good indicators of Γ_0 (hence $R_{\rm dec}$). In particular, the latter correlation can be translated to

$$\Gamma_0 \simeq 195 E_{\gamma,\rm iso,52}^{0.27}, \quad (19)$$

which can be very useful to understand GRB physics (see below).

5. DISCUSSION

5.1. *Implications for Γ_0 measurements and the $\Gamma_0 - E_{\gamma,\rm iso}$ correlation*

Using a sample of GRBs that show the afterglow onset feature in the early optical/X-ray afterglow lightcurves, we manage to constrain Γ_0 for a good sample of GRBs which can be used to perform a statistical study of Γ_0 for the first time. Using a different method (the opacity constraint), the Fermi team recently sets the lower limits of Γ_0 for a number of bright LAT GRBs, e.g. $\Gamma_{0,\rm min} \sim 800$ for GRB 080916C (Abdo et al. 2009a), $\Gamma_{0,\rm min} \sim 1200$ for GRB 090510 (Abdo et al. 2009b), and $\Gamma_{0,\rm min} \sim 1000$ for GRB 090912B (Abdo et al. 2009c). For GRB 080916C, one has $E_{\gamma,\rm iso} \simeq 8.8\times10^{54}$ erg (Abdo et al. 2009a), which corresponds to $\Gamma_0 \sim 1210$ according to the $\Gamma_0 - E_{\gamma,\rm iso}$ relation (Eq.[19]). This is consistent with the lower limit derived by Abdo et al. (2009a). For GRB 090902B, one has $E_{\gamma,\rm iso} \simeq 3.63 \times 10^{54}$ erg (Abdo et al. 2009c), which corresponds to $\Gamma_0 \sim 960$, which is smaller than $\Gamma_{0,\rm min}$ derived by the Fermi team. However, as discussed in the introduction, we believe that this is due to that the Fermi team did not use the most conservative method to derive $\Gamma_{0,\rm min}$. Since GRB 090902B clearly shows a distinct non-thermal component extending to high energy which clearly has a different origin from the MeV component (and very likely from different emission regions, A. Pe'er et al. 2010, in preparation). One should have used the maximum photon energy of the MeV component to estimate $\Gamma_{0,\rm min}$, which would lead to a consistent result with the prediction of the $\Gamma_0 - E_{\gamma,\rm iso}$ relation. For the LAT short GRB 090510, one has $E_{\gamma,\rm iso} = 3.5 \times 10^{52}$, which corresponds to $\Gamma_0 \sim 270$ from the $\Gamma_0 - E_{\gamma,\rm iso}$ relation. This is significantly smaller than $\Gamma_{0,\rm min} = 1200$ set by the 31 GeV photon detected during the first second. Assuming an external shock origin of the GeV emission, Ghirlanda et al. (2009) even derived $\Gamma_0 \sim 2000$ for this burst. The inconsistency is significant. This can be again due to the non-conservative approach of the Fermi team (since the 31 GeV photon is from a different component), but more probably it could be that short GRBs do not satisfy the $\Gamma_0 - E_{\gamma,\rm iso}$ relation derived for long GRBs.

With $\Gamma_0 = 100 - 1200$ derived from the $\Gamma_0 - E_{iso,\gamma}$ relation, we expect that the corresponding observed t_p is in the range of $30 \sim 1400$ seconds for a typical redshift $z = 2$ according to the $\Gamma_0 - t_{p,z}$ correlation (Eq.[17]). In this time period, the observed X-rays are generally dominated by the GRB tail emission or flares. This may be, at least partially, the reason why not many early X-ray lightcurves show the clear afterglow onset bump signature.

The $\Gamma_0 - E_{\gamma,\rm iso}$ relation is very useful to pin down the prompt emission physics of GRBs. One interesting observational correlation is the Amati relation, i.e. $E_p \propto E_{\gamma,\rm iso}^{\kappa}$ (or $E_p \propto L_{\gamma,iso}^{\kappa}$, with $\kappa \sim (0.4 - 0.5)$, both as a bulk correlation among bursts and an internal correlation within a burst (Amati et al. 2002; Wei et al. 2003; Liang et al. 2004; Yonetoku et al. 2004; Lu & Liang 2009). However, all the prompt GRB emission models predict E_p as a function of both $E_{\gamma,\rm iso}$ (or $L_{\gamma,iso}$) and Γ_0 (e.g. Table 1 of Zhang & Mészáros 2002). There is no straightforward theory that predicts the relationship between Γ_0 and $E_{\gamma,\rm iso}$ (or $L_{\gamma,iso}$). As a result, any theoretical model can be argued to interpret the Amati relation, given a designed $\Gamma_0 - E_{\gamma,\rm iso}$ correlation. The $\Gamma_0 - E_{\gamma,\rm iso}$ correlation discovered here therefore poses great constraints on many prompt emission models. For example, the internal shock synchrotron model predicts $E_p \propto L^{1/2}\Gamma_0^{-2}$ (Zhang & Mészáros 2002). The Amati relation essentially requires that $\Gamma_0 \propto L^0$. The $E_p \propto E_{\gamma,\rm iso}^{0.27}$ relation, combined with the trivial proportionality $L \propto E_{\gamma,\rm iso}$ (a non-correlation between GRB duration and luminosity), would lead to $E_p \propto E_{\gamma,\rm iso}^{1/2} E_{\gamma,\rm iso}^{-0.54} \propto E_{\gamma,\rm iso}^{-0.04}$, which means that E_p is essentially constant for different $E_{\gamma,\rm iso}$ values. This is in contradiction with the Amati relation, which can be regarded as another argument against the internal shock synchrotron emission model of GRB prompt emission (see also Kumar & McMahon 2008; Zhang & Pe'er 2009).

5.2. *Early Optical vs. X-ray emission: different physical origins?*

The simultaneous observations in the optical and X-ray bands during the early afterglow phase also hold the key to address whether the broad band emission is from the same emission component. With the prompt slewing capability, the X-ray Telescope (XRT, Burrows et al. 2004) on board Swift has established a large sample of X-ray afterglow of GRBs. Generally, the XRT lightcurves are composed of a few power-law decaying segments and some erratic flares. Although the X-ray lightcurves are diverse among bursts, they can be roughly classified into three groups with a large, uniform sample established by XRT. The majority is the so-called canonical XRT lightcurves characterized by a steep-shallow-normal-steep decay pattern (Zhang et al. 2006; Nousek et al. 2006; O'Brien et al. 2006), although not all the segments show up in every burst (Evans et al. 2009). The second group is composed of those lightcurves that show a single power-law decay from early to late epochs (Liang et al. 2009; Evans et al. 2009). The third group includes some GRBs that show an "internal plateau" that is followed by a rapid drop with a decay slope steeped than -3 (Liang et al. 2007; Troja et al. 2007; Lyons et al. 2009). The physics origin of the X-ray emission is still a mystery (e.g. Zhang 2007 for a review), although the consensus is that there might be diverse origins (Liang et al. 2007). It is clear that the X-ray flares and internal plateaus are of an internal origin. However the origin of the canonical lightcurve is still subject to debate. "Closure"-relation analyses suggest that the normal decay segment following the shallow decay one in the canonical XRT lightcurves are roughly consistent with the forward shock models (Willingale et al. 2007; Liang et al. 2007), favoring the long lasting energy injection models for the shallow-decay segment. However, the optical/X-ray chromatic behavior around the shallow and normal decay transition time (Panaitescu et al. 2006; Fan & Piran 2006; Liang et al.

2007) suggests that the X-ray and optical emissions are two independent components. Some models attribute the entire X-ray emission to the late emission from the central engine, probably related to the long-term accretion history of the central engine (Ghisellini et al. 2007; Kumar et al. 2008; Cui et al. 2009; Cannizzo & Gehrels 2009), but the consistency with the "closure-relation" of the external shock model predictions is not naturally explained in these models. Interestingly, Yamazaki (2009) recently suggested that the X-ray emission might be an independent component prior to the GRB trigger, and that the apparent shallow-to-normal transition is merely reference time effect. Liang et al. (2009) systematically studied the Swift canonical GRB lightcurves and confirm that shifting the reference time can indeed stretch the canonical lightcurves to single power law lightcurves, and proposed a unified picture for the physical origin of both the canonical and the single power-law decaying XRT lightcurves.

As shown in Figure 1, the optical and X-ray lightcurve behaviors are dramatically different at the early epoch, i.e., $t < 1000$ seconds post the GRB trigger. This strongly suggests that the radiations from the two energy bands are not from the same component. The tight correlations between the observables of the prompt gamma-rays and early optical afterglows shown in Fig. 5 strongly suggest that the optical emission is likely the "afterglow" of the GRB fireball (external shock component). This is consistent with the smooth afterglow onset feature observed in the optical band for these GRBs. On the other hand, it also suggests that the early bright X-ray emission is not from the external shock. One natural question would be: where is the external shock X-ray component? Inspecting the details of the X-ray and optical afterglow lightcurves in Figure 1, we can see that this component is very likely hidden underneath some brighter X-ray emission components in the early epochs (e.g. flares, internal plateaus, or even normal plateaus). Interestingly, one can find an X-ray decay slope similar to that of optical in the late epochs in half of GRBs in our sample, including GRBs 050820A, 060418, 060605, 061007, 070318, 070411, 071031, 080319C, 080810, 081203, and 090102. We therefore cannot exclude the possibility that the late X-ray and optical emissions share the same external shock origin.

The mixture of different emission components in the X-ray observations (Willingale et al. 2007; Liang et al. 2007; Liang et al. 2009; Nardini et al. 2009) also naturally interprets the fact that the rarity of the onset afterglow feature observed in the X-ray band. This requires that other early X-ray components are not bright enough to outshine the external shock component. In fact, we find only 13 out of ~ 400 cases in the current XRT lightcurve sample. They are shown in Figure 2. Since the optical band is less affected by the other emission components related to the central engine, one naively expects that the X-ray onset cases should have achromatic optical onset feature as well. Unfortunately, the optical/X-ray joint observations in this sample are rare: only GRB 080507 and GRB 080319C have early optical observations. The optical lightcurve of GRB 080507 is sparse. For GRB 080319C one indeed observes an achromatic onset feature. There is an earlier decay feature in the optical lightcurve of GRB 080319C. It may be associated with an internal emission component within such an interpretation.

6. CONCLUSIONS

We have made an extensively search for the afterglow onset "bump" feature from early afterglow lightcurves, both in the optical band (through literature survey) and in the X-ray band (through systematically analyzing the Swift XRT data). Twenty GRBs are identified in the optical-selected sample and 12 GRBs are found in the X-ray-selected sample. We fit the onset bumps with a smooth broken power-law and measure their characteristics. The rising index r for most bursts is $1-2$, and the decay index d is $0.44-1.77$. These are well consistent with the forward shock models. The peak time t_p is in 10^2-10^3 seconds with a median value of ~ 380 seconds. The width of the bumps measured at FWHM is 10^2-10^3 seconds, and the typical rising time t_r and decaying time t_d are 10^2 seconds and 10^3 seconds, respectively. The ratio of t_r/t_d is narrowly distribution around $0.1-0.3$, and the ratio t_r/t_p has a distribution in the range of $0.3-1$.

Most GRBs in our optical-selected sample have redshift measurements. We analyze pair correlations among the bump characteristics. We find that the pulse width, rising time, decaying time, and the peak time are strongly correlated. Bumps that peak later are dimmer and wider. No correlation between the decay index d with other parameters is found, but the rising index r is tightly anti-correlated with both the ratio t_r/t_d and t_r/t_p, although it is not correlated with t_r and t_d.

We analyze the relation of the optical afterglow bumps with prompt gamma-ray properties. We find that a GRB with larger $E_{\gamma,\rm iso}$ tends to have a brighter optical afterglow, and tends to be decelerated by the surrounding medium earlier. These tight correlations strongly suggests an external shock afterglow origin of the early optical emission.

Within the framework of the standard forward model in a constant density circumburst medium, we calculate the initial Lorentz factor Γ_0 and the deceleration radius $R_{\rm dec}$ for the GRBs in the optical-selected sample. The derived Γ_0 ranges from 100 to about 600, while $R_{\rm dec}$ narrowly distributed around 10^{17} cm.

Intriguingly, we discover a tight correlation between Γ_0 and $E_{\gamma,\rm iso}$. For typical values $n = 1$ cm^{-3} and $\eta = 0.2$ (Γ_0 is insensitive to the values of n and η, we obtain the correlation Eq.(19). This correlation is very important to understand GRB prompt emission physics, and may serve as an indicator of Γ_0 for other long GRBs. In particular, the correlation disfavors the internal shock synchrotron emission model for the GRB prompt emission. The extrapolation of the correlation is consistent with the $\Gamma_{0,\rm min}$ of GRB 080916C derived by the Fermi team (Abdo et al. 2009a), but are inconsistent with the $\Gamma_{0,\rm min}$ of GRB 090510 and GRB 090902B derived by the Fermi team (Abdo et al. 2009b,c). We point out that this is because the Fermi team did not use a more conservative approach to set $\Gamma_{0,\rm min}$.

The X-ray-selected sample only has two cases with redshift measurements. The derived Γ_0's from these two cases are also consistent with the $\Gamma_0 - E_{\gamma,\rm iso}$ correlation derived from the optical-selected sample. There is one case (GRB 080319C) that shows an achromatic afterglow onset feature.

Most optical-selected sample has early X-ray emission components not from the external shock. This reinforces the diverse origin of early X-ray afterglow in most GRBs.

We acknowledge the use of the public data from the Swift data archive. This work is supported by the National Natural Science Foundation of China under grants No. 10873002, the National Basic Research Program ("973" Program) of China (Grant 2009CB824800), the research foundation of Guangxi University (M30520). It is also partially supported by NASA NNX09AT66G and NNX10AD48G, as well as NSF AST-0908362. BBZ acknowledges the President's Fellow Ship and GPSA awards from UNLV.

REFERENCES

Abdo, A. A., et al. 2009a, Science, 323, 1688
Abdo, A. A., et al. 2009b, ApJ, 706, L138
Abdo, A. A., et al. 2009c, arXiv:0908.1832
Amati, L., et al. 2002, A&A, 390, 81
Baring, M. G., & Harding, A. K. 1997, ApJ, 491, 663
Cannizzo, J. K., & Gehrels, N. 2009, ApJ, 700, 1047
Cenko, S. B., Gezari, S., Small, T., Fox, D. B., & Chornock, R. 2007, GRB Coordinates Network, 6322, 1
Cenko, S. B., et al. 2006, ApJ, 652, 490
Chen, H.-W., Prochaska, J. X., Herbert-Fort, S., Christlein, D., & Cortes, S. 2007, GRB Coordinates Network, 6217, 1
Covino, S., et al. 2008, MNRAS, 388, 347
Cucchiara, A. 2008, GRB Coordinates Network, 7547, 1
Cucchiara, A., Fox, D. B., Cenko, S. B., & Price, P. A. 2007, GRB Coordinates Network, 6083, 1
Cui, X.-H., Liang, E.-W., Lv, H.-J., Zhang, B.-B., & Xu, R.-X. 2009, MNRAS, 1643
Evans, P. A., et al. 2009, MNRAS, 397, 1177
Fan, Y., & Piran, T. 2006, MNRAS, 369, 197
Fenimore, E. E., Epstein, R. I., & Ho, C. 1993, A&AS, 97, 59
Fugazza, D., et al. 2006, GRB Coordinates Network, 5513, 1
Ghirlanda, G., Ghisellini, G., & Nava, L. 2009, arXiv:0909.0016
Ghisellini, G., Ghirlanda, G., Nava, L., & Firmani, C. 2007, ApJ, 658, L75
Guidorzi, C., et al. 2009, A&A, 499, 439
Gupta, N., & Zhang, B. 2008, MNRAS, 384, L11
Holland, S. T., & Pagani, C. 2008, GRB Coordinates Network, 7497, 1
Jakobsson, P., Fynbo, J. P. U., Tanvir, N., & Rol, E. 2006, GRB Coordinates Network, 5716, 1
Jakobsson, P., Malesani, D., Thoene, C. C., Fynbo, J. P. U., Hjorth, J., Jaunsen, A. O., Andersen, M. I., & Vreeswijk, P. M. 2007, GRB Coordinates Network, 6283, 1
Jin, Z. P., & Fan, Y. Z. 2007, MNRAS, 378, 1043
Klotz, A., Gendre, B., Atteia, J. L., Boër, M., Coward, D. M., & Imerito, A. C. 2009, ApJ, 697, L18
Klotz, A., et al. 2008, A&A, 483, 847
Kobayashi, S. 2000, ApJ, 545, 807
Kobayashi, S., & Zhang, B. 2007, ApJ, 655, 973
Kocevski, D., & Liang, E. P. 2001, 20th Texas Symposium on relativistic astrophysics, 586, 623
Krühler, T., et al. 2009, A&A, 508, 593
Krühler, T., et al. 2009, ApJ, 697, 758
Kuin, N. P. M., et al. 2009, MNRAS, 395, L21
Kumar, P., Narayan, R., & Johnson, J. L. 2008, Science, 321, 376
Landsman, W., de Pasquale, M., Kuin, P., Schady, P., Smith, P., & Parsons, A. 2008, GRB Coordinates Network, 8601, 1
Ledoux, C., Jakobsson, P., Jaunsen, A. O., Thoene, C. C., Vreeswijk, P. M., Malesani, D., Fynbo, J. P. U., & Hjorth, J. 2007, GRB Coordinates Network, 7023, 1
Ledoux, C., et al. 2005, GRB Coordinates Network, 3860, 1
Ledoux, C., Vreeswijk, P., Smette, A., Jaunsen, A., & Kaufer, A. 2006, GRB Coordinates Network, 5237, 1
Liang, E. W., Dai, Z. G., & Wu, X. F. 2004, ApJ, 606, L29
Liang, E.-W., Lü, H.-J., Hou, S.-J., Zhang, B.-B., & Zhang, B. 2009, ApJ, 707, 328
Liang, E.-W., Racusin, J. L., Zhang, B., Zhang, B.-B., & Burrows, D. N. 2008, ApJ, 675, 528
Liang, E.-W., Zhang, B.-B., & Zhang, B. 2007, ApJ, 670, 565
Lu, R. J., & Liang, E. -W. 2009, Science in China G, 2009, in press
Lyons, N., O'Brien, P. T., Zhang, B., Willingale, R., Troja, E., & Starling, R. L. C. 2009, arXiv:0908.3798
Mészáros, P. 2002, ARA&A, 40, 137
Malesani, D., et al. 2007, GRB Coordinates Network, 6343, 1
Melandri, A., et al. 2009, MNRAS, 395, 1941
Mészáros, P., & Rees, M. J. 1997, ApJ, 476, 232
Mészáros, P., & Rees, M. J. 1993, ApJ, 405, 278
Molinari, E., et al. 2007, A&A, 469, L13
Nardini, M., Ghisellini, G., Ghirlanda, G., & Celotti, A. 2009, arXiv:0908.0734
Nousek, J. A., et al. 2006, ApJ, 642, 389
O'Brien, P. T., et al. 2006, ApJ, 647, 1213
Page, K. L., et al. 2009, MNRAS, 400, 134
Panaitescu, A. 2007, MNRAS, 380, 374
Panaitescu, A., Mészáros, P., Burrows, D., Nousek, J., Gehrels, N., O'Brien, P., & Willingale, R. 2006, MNRAS, 369, 2059
Pandey, S. B., et al. 2006, A&A, 460, 415
Pe'er, A., Ryde, F., Wijers, R. A. M. J., Mészáros, P., & Rees, M. J. 2007, ApJ, 664, L1
Perley, D. A., Chornock, R., & Bloom, J. S. 2008, GRB Coordinates Network, 7962, 1
Peterson, B., & Schmidt, B. 2006, GRB Coordinates Network, 5223, 1
Piran, T. 2004, Reviews of Modern Physics, 76, 1143
Prochaska, J. X., Chen, H.-W., Bloom, J. S., Falco, E., & Dupree, A. K. 2006, GRB Coordinates Network, 5002, 1
Prochaska, J. X., Perley, D., Howard, A., Chen, H.-W., Marcy, G., Fischer, D., & Wilburn, C. 2008, GRB Coordinates Network, 8083, 1
Prochaska, J. X., Perley, D. A., Modjaz, M., Bloom, J. S., Poznanski, D., & Chen, H.-W. 2007, GRB Coordinates Network, 6864, 1
Ramirez-Ruiz, E., & Fenimore, E. E. 2000, ApJ, 539, 712
Rees, M. J., & Meszaros, P. 1994, ApJ, 430, L93
Rol, E., et al. 2005, GRB Coordinates Network, 3710, 1
Roming, P. W. A., et al. 2009, ApJ, 690, 163
Ryde, F., et al. 2009, arXiv:0911.2025
Rykoff, E. S., et al. 2009, ApJ, 702, 489
Rykoff, E. S., et al. 2004, ApJ, 601, 1013
Sari, R. 1997, ApJ, 489, L37
Sari, R., & Piran, T. 1999, ApJ, 520, 641
Sari, R., Piran, T., & Narayan, R. 1998, ApJ, 497, L17
Troja, E., et al. 2007, ApJ, 665, 599
Wei, D. M., & Gao, W. H. 2003, MNRAS, 345, 743
Wiersema, K., Tanvir, N., Vreeswijk, P., Fynbo, J., Starling, R., Rol, E., & Jakobsson, P. 2008, GRB Coordinates Network, 7517, 1
Willingale, R., et al. 2007, ApJ, 662, 1093
Woods, E., & Loeb, A. 1995, ApJ, 453, 583
Xue, R.-R., Fan, Y.-Z., & Wei, D.-M. 2009, A&A, 498, 671
Yamazaki, R. 2009, ApJ, 690, L118
Yonetoku, D., Murakami, T., Nakamura, T., Yamazaki, R., Inoue, A. K., & Ioka, K. 2004, ApJ, 609, 935
Zhang, B.-B., Liang, E.-W., & Zhang, B. 2007, ApJ, 666, 1002
Zhang, B. 2007, Chinese Journal of Astronomy and Astrophysics, 7, 1
Zhang, B., Fan, Y. Z., Dyks, J., Kobayashi, S., Mészáros, P., Burrows, D. N., Nousek, J. A., & Gehrels, N. 2006, ApJ, 642, 354
Zhang, B., & Kobayashi, S. 2005, ApJ, 628, 315
Zhang, B., Kobayashi, S., & Mészáros, P. 2003, ApJ, 595, 950
Zhang, B., & Mészáros, P. 2004, International Journal of Modern Physics A, 19, 2385
Zhang, B., & Mészáros, P. 2002, ApJ, 581, 1236
Zhang, B., & Pe'er, A. 2009, ApJ, 700, L65
Zou, Y.-C., & Piran, T. 2009, MNRAS, 1788

TABLE 1
Optical observations and fitting result for our sample

GRB(Band)	z^{Ref}	F_m[a]	t_p[a]	α_1	α_2	χ^2/dof	w[a]	t_r[a]	t_d[a]	t_r/t_d	t_r/t_p	Refs.
030418(V)	...	2.51±0.06	1344.5±78.6	1.17±0.20	0.74±0.08	26/9	5816	953	4863	0.20	0.71	(18)
050730(V)	3.97(1)	4.00±0.45	590.7±131.5	1.36±0.43	1.02±0.15	25/7	1836	339	1497	0.23	0.57	(19)
050820A(R)	2.615(2)	21.10±1.25	391.0±16.7	4.45±0.76	1.04±0.01	47/7	711	120	592	0.20	0.31	(20)
060418(H)	1.49(3)	88.70±1.71	153.3±3.3	2.70±0.22	1.27±0.02	16/8	298	65	233	0.28	0.42	(21)
060605(R)	3.8(4)	9.59±0.20	399.1±13.0	0.90±0.09	1.17±0.05	74/50	1313	281	1032	0.27	0.70	(22)
060607A(H)	3.082(5)	28.60±0.49	180.9±2.4	4.15±0.22	1.32±0.04	46/23	259	57	202	0.28	0.31	(21)
060904B(V)	0.703(6)	4.91±0.29	467.9±48.4	1.56±0.43	0.85±0.22	15/13	1524	281	1243	0.23	0.60	(23)
061007(R)	1.262(7)	1820.0±12.0	78.3±0.4	2.17±0.04	1.71±0.01	811/79	142	31	111	0.28	0.39	(22)
070318(V)	0.84(8)	14.20±0.43	301.0±21.3	1.05±0.14	1.12±0.05	9/6	1090	233	857	0.27	0.77	(24)
070411(R)	2.954(9)	3.74±2.60	450.1±5.0	0.76±0.03	1.54±0.03	754/17	1603	359	1243	0.29	0.80	(25)
070419A(R)	0.97(10)	0.46±0.01	587.0±20.9	2.20±0.24	1.27±0.04	102/43	1387	239	1148	0.21	0.41	(26)
070420(R)	...	12.80±1.10	213.2±18.7	2.59±1.07	1.10±0.33	4/4	433	94	339	0.28	0.44	(23)
071010A(R)	0.98(11)	3.90±0.26	368.2±24.4	2.36±0.43	0.74±0.01	12/20	1234	202	1032	0.20	0.55	(27)
071031(R)	2.692(12)	0.71±0.01	1018.6±1.6	1.11±0.01	0.92±0.01	9819/22	4009	657	3352	0.20	0.65	(28)
080319C(N)	1.95(13)	2.57±0.03	338.3±5.6	2.00(fixed)	1.50(fixed)	22/4	628	137	491	0.28	0.40	(29)
080330(R)	1.51(14)	1.43±0.02	621.9±17.0	0.34±0.03	1.77±0.12	30/36	3552	632	2920	0.22	1.02	(30)
080710(R)	0.845(15)	3.31±0.03	2200.9±4.1	1.34±0.01	0.97±0.01	2511/61	6754	1245	5508	0.23	0.57	(31)
080810(R)	3.35(16)	107.00±1.70	117.6±1.1	1.34±0.04	1.21±0.01	854/62	344	85	259	0.33	0.72	(32)
081126(R)	...	12.70±0.20	201.3±1.2	2.04±0.06	0.44±0.01	244/5	1330	134	1197	0.11	0.66	(33)
081203A(U)	2.1(17)	110.00±0.20	367.1±0.8	2.09±0.01	1.49±0.01	3176/32	794	202	592	0.34	0.55	(34)

References. — (1) Rol et al.(2005); (2) Ledoux et al.(2005); (3) Prochaska et al.(2006); (4) Peterson et al.(2006); (5) Ledoux et al.(2006); (6) Fugazza et al.(2006); (7) Jakobsson et al.(2006); (8) Chen et al.(2007); (9) Jakobsson et al.(2007); (10) Cenko et al.(2007); (11) Prochaska et al.(2007); (12) Ledoux et al.(2007); (13) Wiersema et al.(2008); (14) Cucchiara (2008); (15) Perley et al.(2008); (16) Prochaska et al.(2008); (17) Landsman et al.(2008); (18) Rykoff et al.(2004); (19) Pandey et al.(2006); (20) Cenko et al.(2007); (21) Molinari et al.(2007); (22) Rykoff et al.(2009); (23) Klotz et al.(2008); (24) Roming et al.(2009); (25) Malesani et al.(2007); (26) Melandri et al.(2009); (27) Covino et al.(2008); (28) Krühler et al.(2009); (29) Holland et al.(2008); (30) Guidorzi et al.(2009); (31) Krühler et al.(2009); (32) Page et al.(2009); (33) Klotz et al.(2009); (34) Kuin et al.(2009)

[a] In units of 10^{-12}erg cm^{-2} s^{-1}.
[b] In units of seconds.

TABLE 2
XRT observations and fitting result for our sample

GRB	z^{Ref}	F_m [a]	t_p[b]	α_1	α_2	χ^2(dof)	ω	t_r[b]	t_d[b]	t_r/t_d	t_r/t_p
060319	...	8.46±0.98	267.0±20.2	5.46±2.05	1.13±0.04	43/30	490	82	408	0.20	0.31
060801	...	20.20±3.50	114.3±9.5	6.69±4.42	1.77±0.27	3/6	134	39	94	0.42	0.34
060804	...	7.60±0.66	418.9±176.1	0.85±0.67	1.22±0.07	25/23	1603	281	1322	0.21	0.67
070103	...	1.60±0.13	685.5±64.3	0.76±0.16	1.47±0.08	22/24	2325	521	1803	0.29	0.76
070208	1.165(1)	1.80±0.29	968.1±72.9	1.09±0.27	1.29±0.06	39/30	3274	657	2616	0.25	0.68
070714A	...	1.38±0.24	234.0±36.9	2.25±1.46	0.86±0.12	16/8	685	94	591	0.16	0.40
080307	...	67.10±1.50	210.5±3.12	2.22±0.16	2.05±0.04	141/153	338	94	244	0.39	0.45
080319C	1.95(2)	58.40±3.50	432.8±29.1	1.55±0.41	1.41±0.03	72/52	994	281	713	0.39	0.65
080409	...	0.78±0.08	395.9±100.0	0.50±0.00	1.11±0.11	13/10	2007	336	1671	0.20	0.85
090429B	...	1.52±0.14	540.2±51.6	1.57±0.38	1.34±0.08	15/13	1487	339	1148	0.29	0.63
090607	...	40.40±2.50	118.9±3.48	4.86±1.13	2.79±0.39	25/20	134	39	94	0.42	0.33

References. — (1) Cucchiara et al.(2007); (2) Prochaska et al.(2007); (3) Wiersema et al.(2008)

[a] In units of 10^{-11}erg cm^{-2} s^{-1}.
[b] In units of seconds.

TABLE 3
The optical and X-ray with know redshift in our sample

GRB	z	$E_{\rm iso,\gamma}$ (10^{52} erg)	$L_{\rm p}$ (10^{47} erg/s)	$E_{\rm iso,O}$ (10^{48} erg)	Γ_0	$R_{\rm d}$ (10^{17}cm)
Optical						
050730	3.97	13.37±1.22	166.42	6.04±0.68	306±26	1.67
050820A	2.615	2.92±0.31	170.74	11.72±0.69	262±5	1.11
060418	1.49	4.68±0.14	111.23	12.42±0.24	344±3	1.09
060605	3.8	1.98±0.26	274.19	13.05±0.27	276±6	0.95
060607A	3.082	5.25±0.20	114.90	23.56±0.40	394±3	1.03
060904B	0.703	0.21±0.02	7.18	0.11±0.01	133±5	0.73
061007	1.262	75.96±4.93	800.64	168.6±1.12	603±5	1.89
070318	0.84	0.46±0.02	20.78	0.48±0.01	178±5	0.78
070411	2.954	5.09±0.30	83.64	2.78±0.02	276±2	1.3
070419A	0.97	0.14±0.02	1.13	0.02±0.006	122±3	0.67
071010A	0.98	0.05±0.01	8.67	0.19±0.01	129±5	0.46
071031	2.692	1.45±0.21	33.26	0.42±0.03	169±3	1.18
080319C	1.95	13.8±3.13	11.55	0.70±0.01	311±9	1.67
080330	1.51	0.20±0.05	21.24	0.21±0.003	137±4	0.70
080710	0.845	0.26±0.04	31.70	0.11±0.001	79±1	1.11
080810	3.35	39.37±2.32	629.20	107.6±1.71	610±5	1.51
081203A	2.1	8.08±0.31	666.19	35.66±0.08	288±1	1.47
X-ray						
070208	1.165	0.16±0.04	1.40±0.12	194.6	102±3	0.79
080319C	1.95	3.31±0.09	162±8	3772.5	242±4	1.23

TABLE 4
Spearman correlation coefficients of the Optical Selected Sample

	$L_{\rm p,O}$	$t_p{}'$	r	d	$t_r{}'$	$t_d{}'$	t_r/t_d	t_r/t_p	w'
$L_{\rm p,O}$		-0.90	X	X	-0.89	-0.88	X	X	-0.88
$t_p{}'$			X	X	0.95	0.93	X	X	0.94
r				X	X	X	0.90	0.90	X
d					X	X	X	X	X
$t_r{}'$						0.98	X	X	0.98
$t_d{}'$							X	X	~ 1
t_r/t_d								X	X
t_r/t_p									X

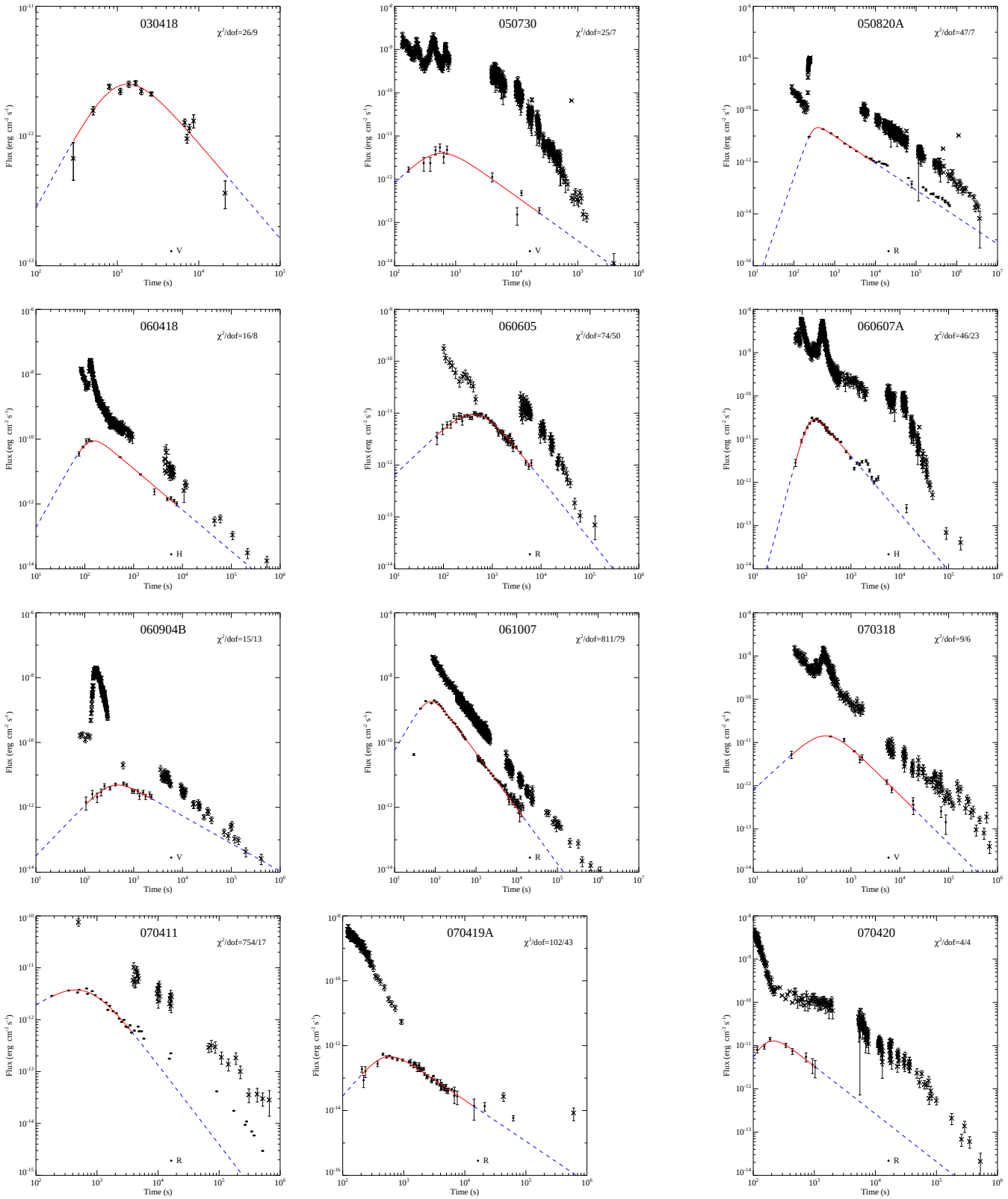

FIG. 1.— Lightcurves of the optical-selected sample (dots). Lines are the best fits with a smooth broken power-law to the optical data in a selected interval marked as a red *solid* segment. Blue *dashed* segments just extend the fitting curves in a broad time regime. The simultaneous X-ray data observed with *Swift*/XRT (crosses with error bands) are also present.

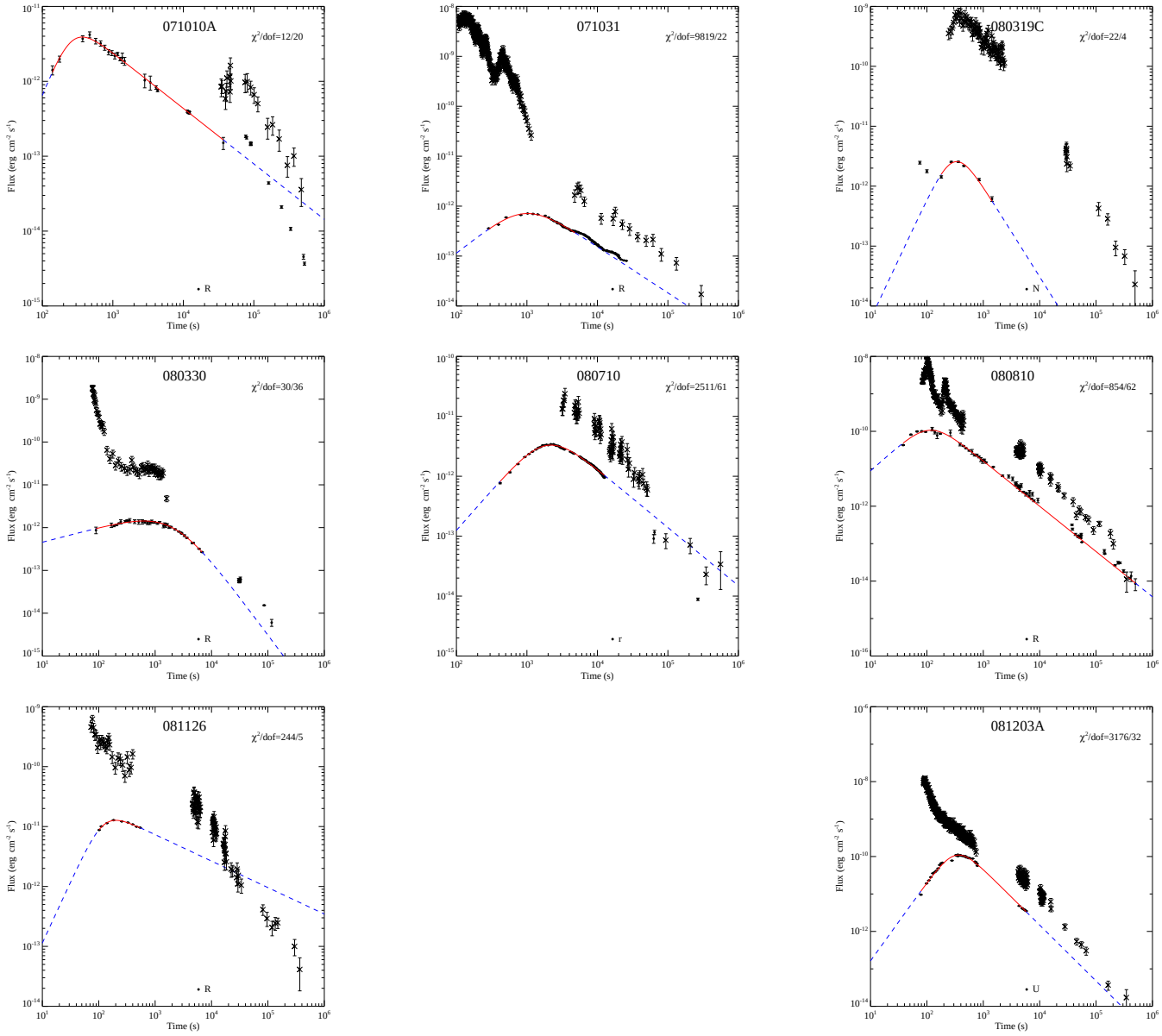

Fig. 1— continued

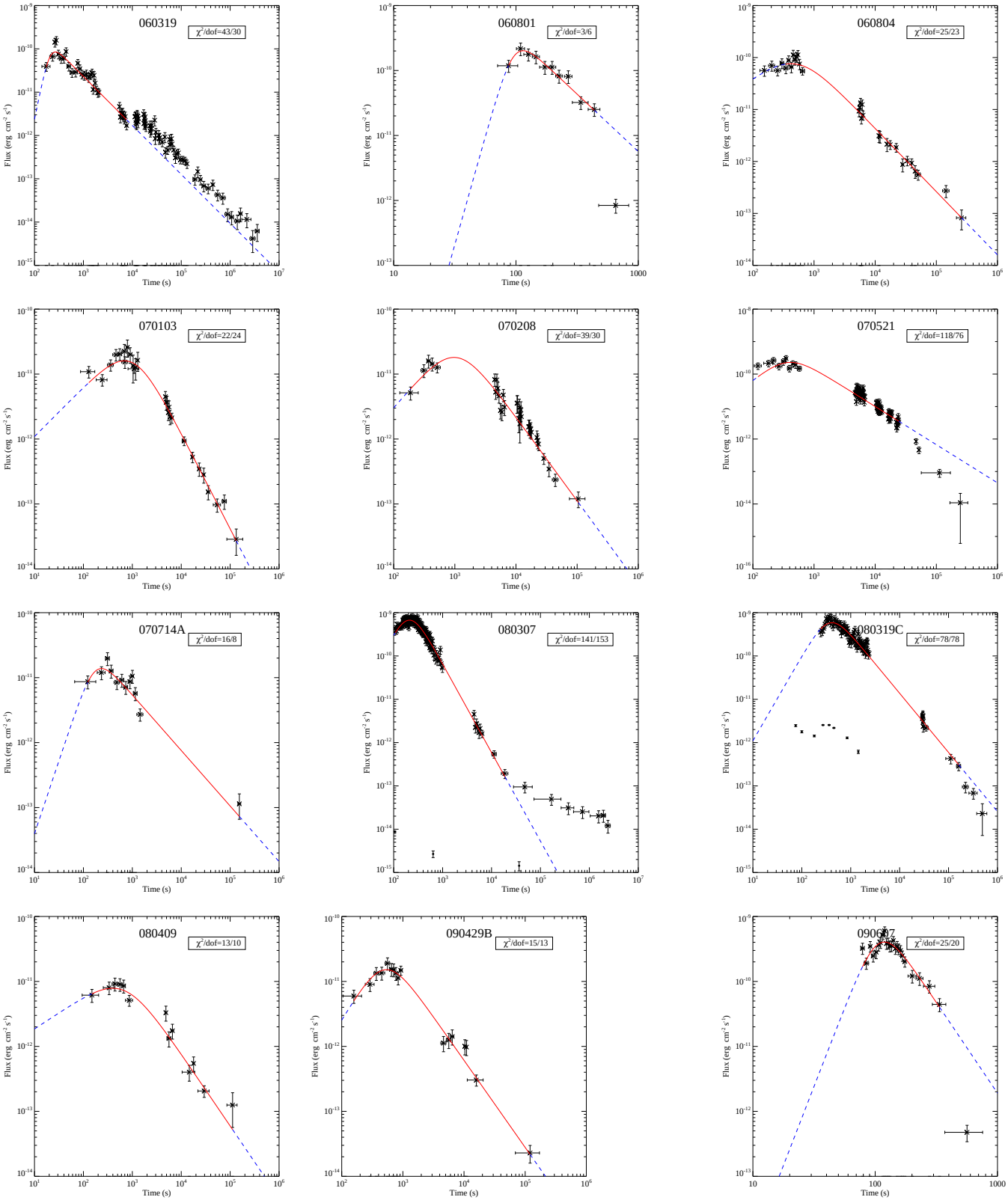

FIG. 2.— The same as Figure 1, but for the X-ray selected sample.

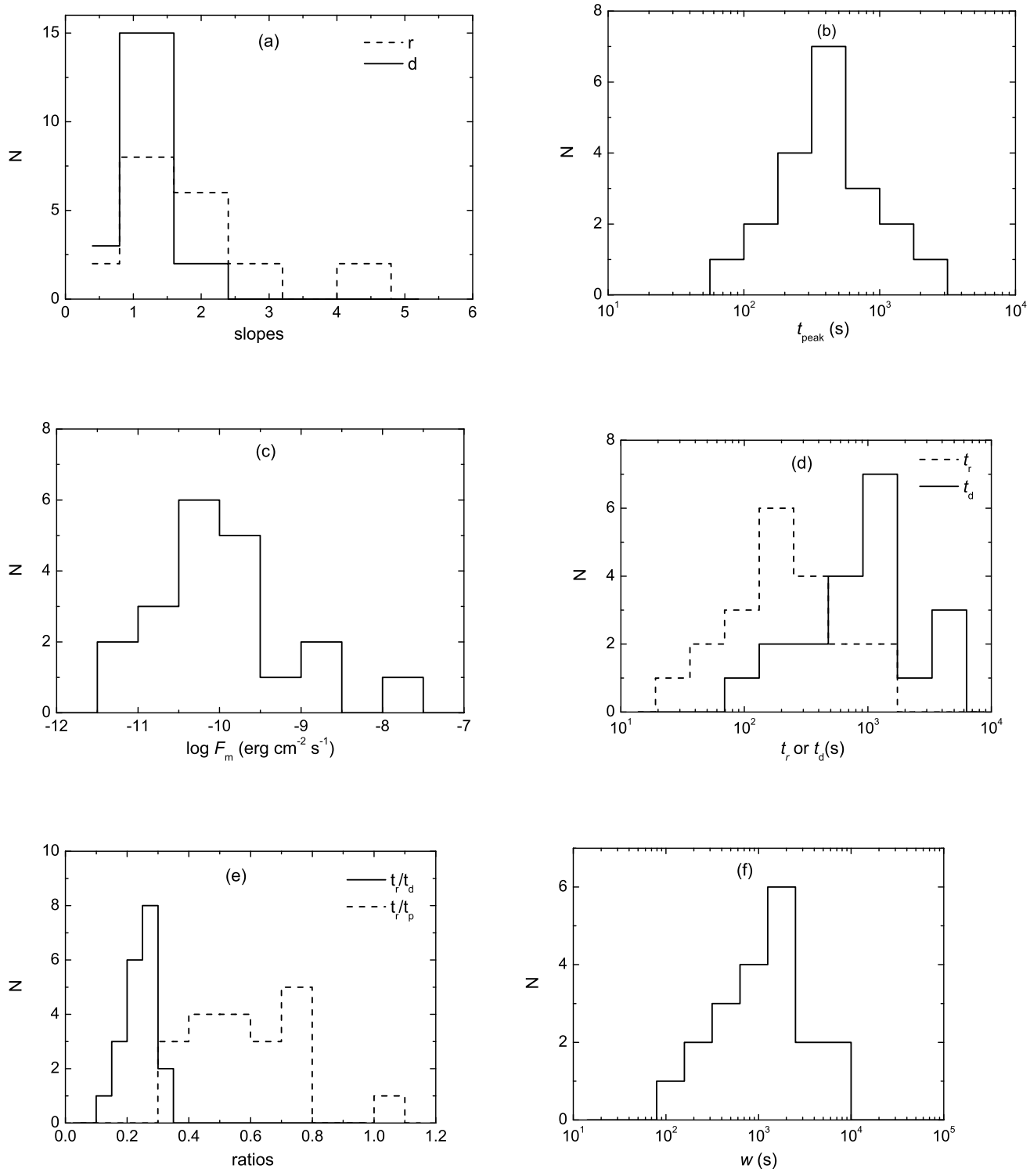

FIG. 3.— Distributions of the characteristics of the optical-selected sample.

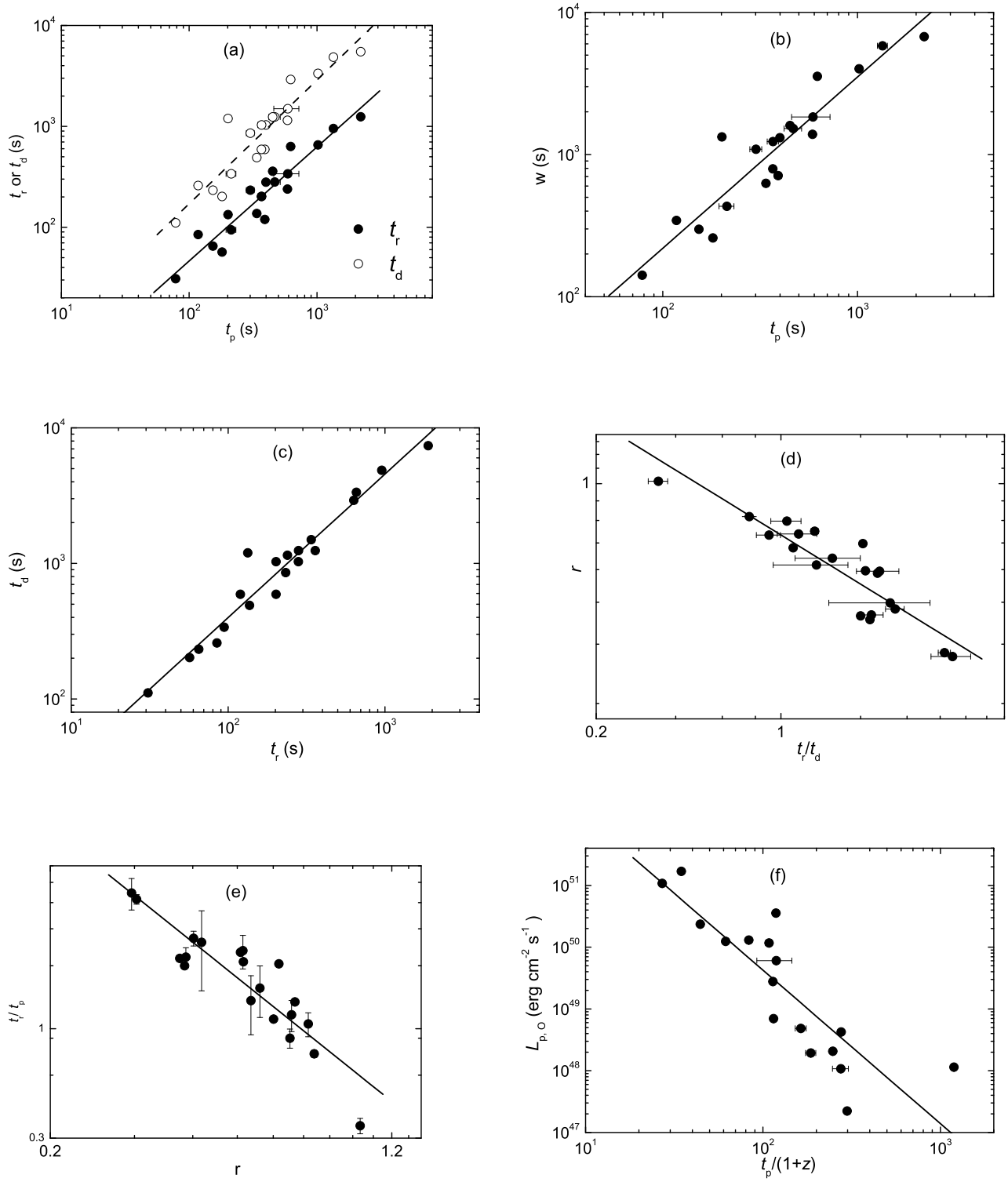

FIG. 4.— Pair correlations among the characteristics of the optical-selected sample. Lines are the best fits.

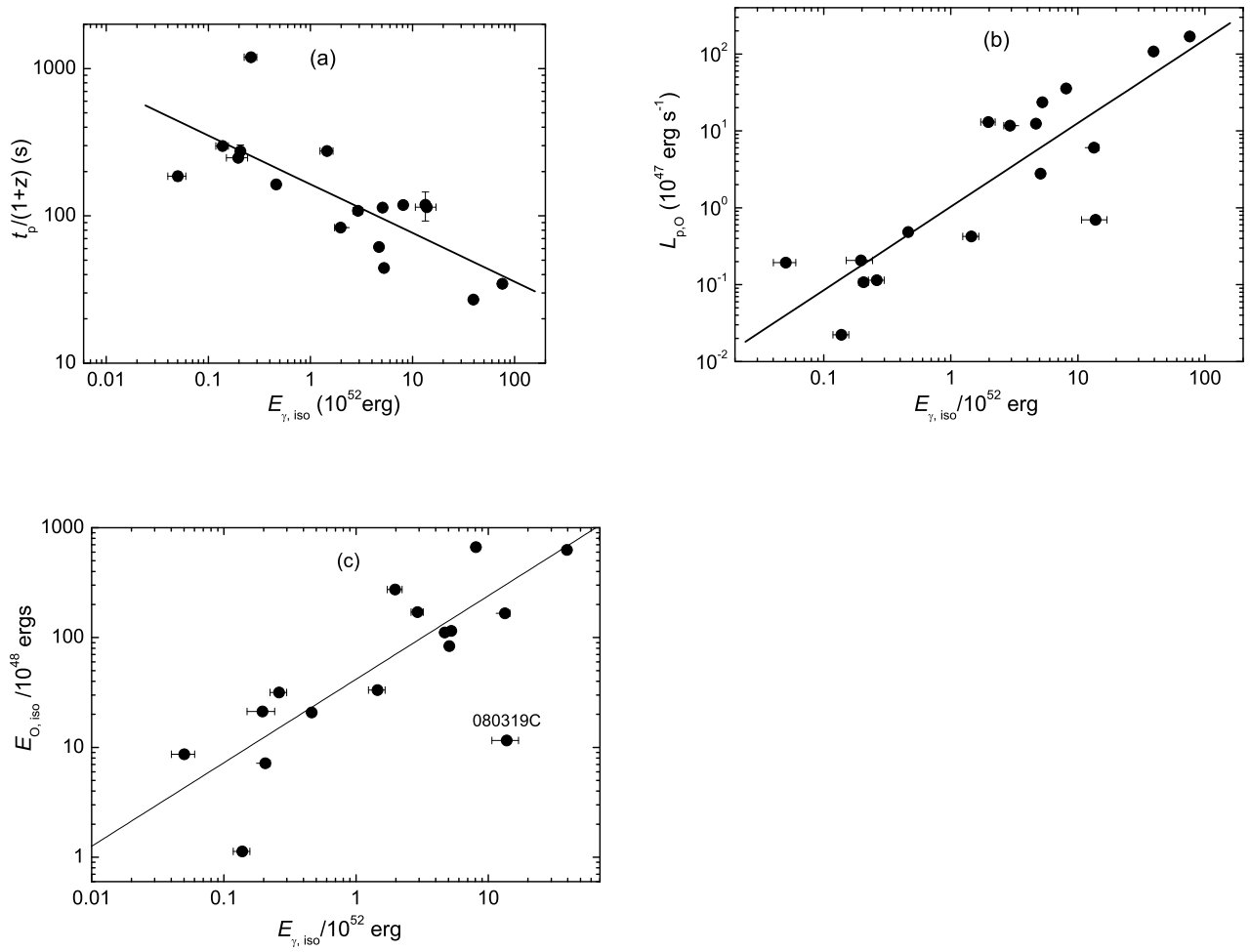

FIG. 5.— Relations of $E_{\rm iso,\gamma}$ to $t_p/(1+z)$, $L_{p,O}$ and $E_{\rm iso,O}$ for the optical selected sample. Lines are the best fits.

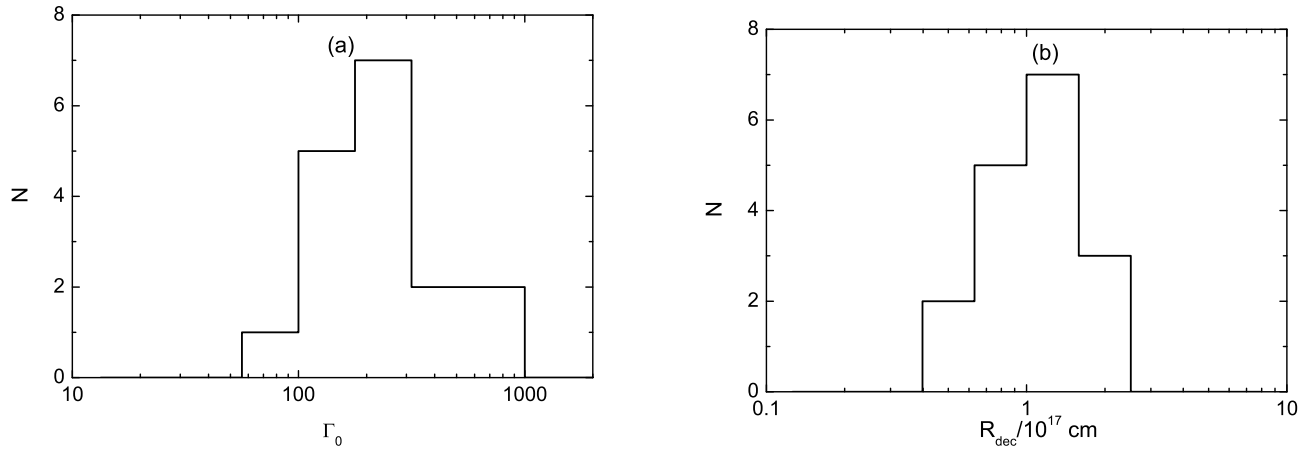

FIG. 6.— Distributions of Γ_0 and R_d for the optical-selected sample

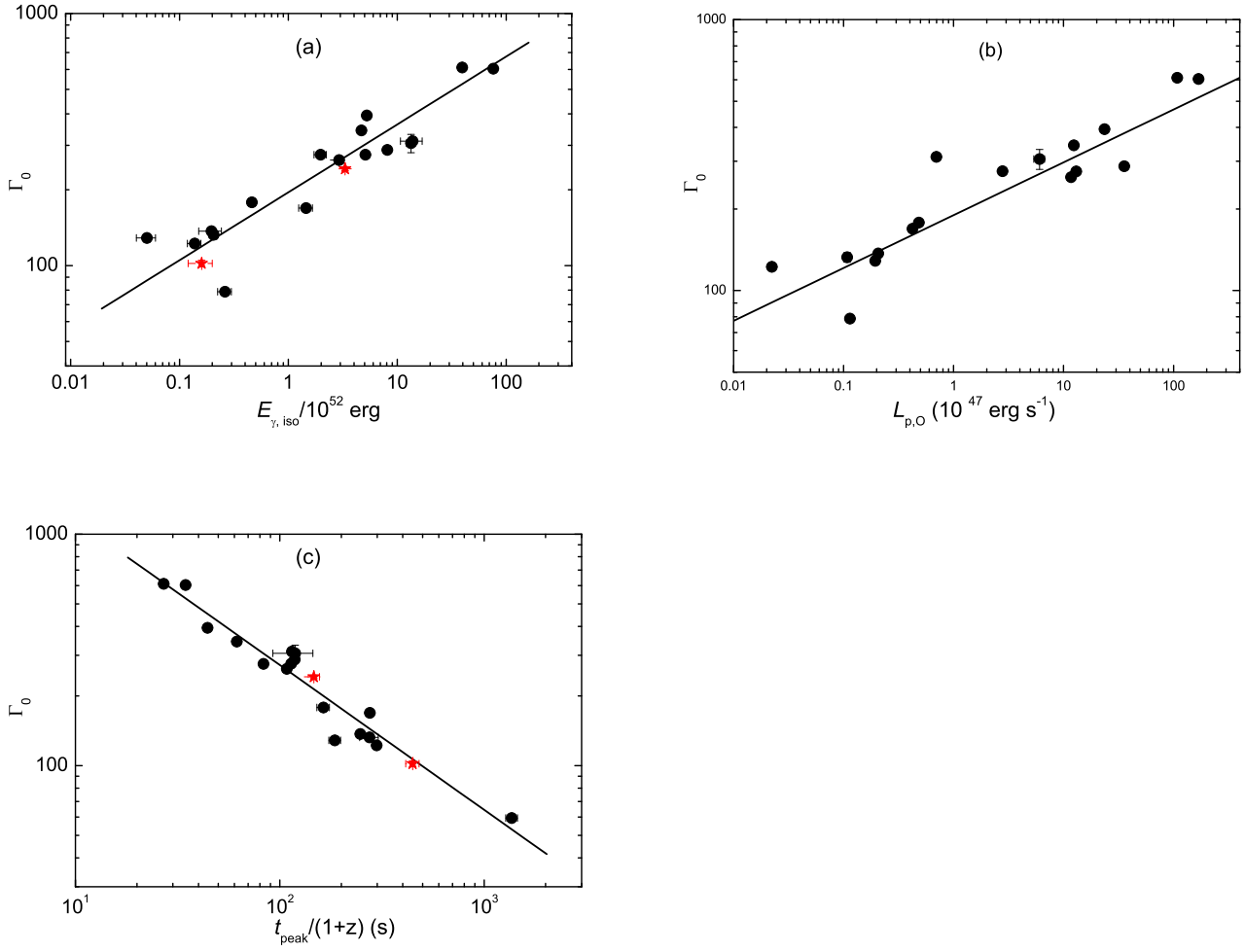

FIG. 7.— Relations of Γ_0 to $E_{\rm iso,\gamma}$, $L_{\rm p,O}$, and $t_p/(1+z)$. Lines are the best fits for the optical-selected sample. GRBs 070208 and 080319C in the X-ray selected sample have redshift measurement. We mark the two GRBs with red stars.

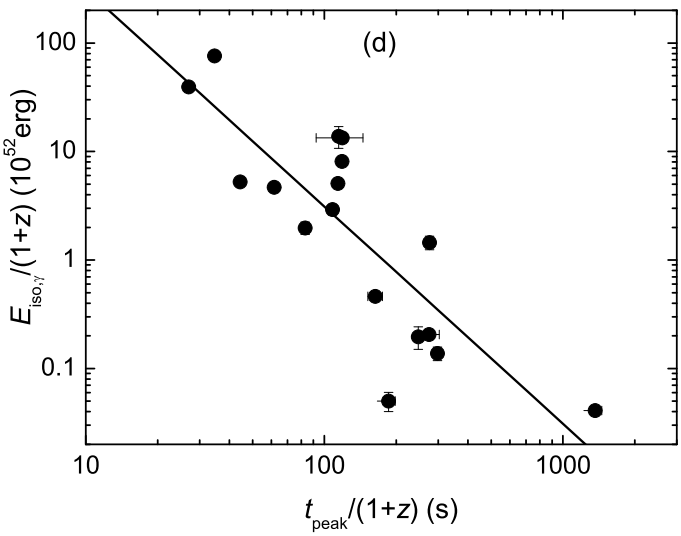
(d)
100
10
1
0.1
10
100
1000
$E_{iso,\gamma}$/(1+z) (10^{52}erg)
t_{peak}/(1+z) (s)